International Journal of Non-Linear Mechanics 113 (2019) 55–61

Contents lists available at ScienceDirect

International Journal of Non-Linear Mechanics

journal homepage: www.elsevier.com/locate/nlm

Properties of impact events in the model of forced impacting oscillator: Experimental and numerical investigations

Sergii Skurativskyi [a], Grzegorz Kudra [b,*], Grzegorz Wasilewski [b], Jan Awrejcewicz [b]

[a] Subbotin Institute of Geophysics, NAS of Ukraine, Kyiv, Ukraine
[b] Lodz University of Technology, Department of Automation, Biomechanics and Mechatronics, Lodz, Poland

ARTICLE INFO

Keywords:
Forced oscillator
Bifurcations
Impact
Spike statistics
Chaos

ABSTRACT

The paper deals with the studies of the forced impacting oscillator when taking into account the dry and viscous resistance as well as the generalized Hertz contact law during an impact. Numerical investigations of the mathematical model are accompanied by validations obtained with an experimental rig. To study the solutions of the mathematical model, the sequences of impacts, when the system evolves in periodic and chaotic modes, is used. The statistical properties of chaotic impact events are considered in detail. In particular, successive iterations of the impact map, autocorrelation function and coefficient of variation for the impact train, histograms for the inter-impact intervals and values of obstacle penetrations are analyzed. It is revealed that the impact sequence is stationary but non-Poissonian and contains temporal scales that do not relate to the external stimulus. This sequence can be described by a bimodal distribution. The findings are confirmed by the analysis of experimental data.

0. Introduction

Impacts phenomena are diverse and widely encountered in mechanical systems. The studies of such systems can be realized within the framework of nonsmooth dynamical models [1,2] where the limiters of motion are introduced. Due to nonsmoothness, the consideration of these mathematical models can lead to the class of strongly nonlinear models characterized by special behaviors [2–5].

As it has been shown in a wide range of works [6–9], impacting systems subjected to external excitation possess harmonic, subharmonic, chaotic and other complicated motions. The bifurcation phenomena both specific (i.e., various types of grazing bifurcations [10,11]) and such that are inherent in smooth systems [12] take place when the control parameters are varied. To date, the general foundations of one-degree-of-freedom impacting systems, their theoretical description and experimental validation have been developed essentially.

However, the peculiarities of the impacting system in the case of presence of multiperiodic or chaotic regimes are still poorly investigated. To deeper understand the nature of complicated regimes, it can be useful to analyze the sets of discrete events extracted from the system's dynamics. Events or spikes, as they are referred to by neuroscientists [13], can be identified as abrupt changes in the system variable [14]. To generate spike sequences, as a rule, the threshold-crossing and integrate-and-fire techniques [15,16] are employed. In the case of an impacting system, a natural threshold (i.e., a limiter) is present. When the system trajectory crosses the level defined by the limiter, the temporal moments of impacts form the impacting map [17], statistical properties of which are extremely interesting (especially in chaotic modes).

It should be noted that impact sequences can be associated with Poincaré sections, which are simply defined in the case of harmonic external loading. As for the advantages of impact sequences [18], let us consider the situation when the loading is unharmonic. In such a case, the Poincaré section technique for nonautonomous models requires some modifications, whereas the studies of impacts can be carried out in the same manner as in the case of harmonic excitation. Moreover, inter-impact intervals allow one to assess the dynamical and geometrical properties of chaotic attractors [19].

Impact events (as well as the displacement or velocity of a cart) are part of information directly produced by the oscillating system. The searching for regularities hidden in this information motivates us to consider discrete event sequences and develop proper tools for these purposes.

The present paper is organized as follows. In Section 1, we describe the experimental rig and the corresponding mathematical model. Some previously obtained results regarding the validation of the model and the bifurcation scenario are presented as well. In Section 2, the construction of impact trains and their statistical analysis are described. The final section contains the concluding remarks.

* Corresponding author.
E-mail addresses: skurserg@gmail.com (S. Skurativskyi), grzegorz.kudra@p.lodz.pl (G. Kudra), grzegorz.wasilewski@p.lodz.pl (G. Wasilewski), jan.awrejcewicz@p.lodz.pl (J. Awrejcewicz).

https://doi.org/10.1016/j.ijnonlinmec.2019.03.013
Received 2 January 2019; Received in revised form 1 March 2019; Accepted 25 March 2019
Available online 27 March 2019

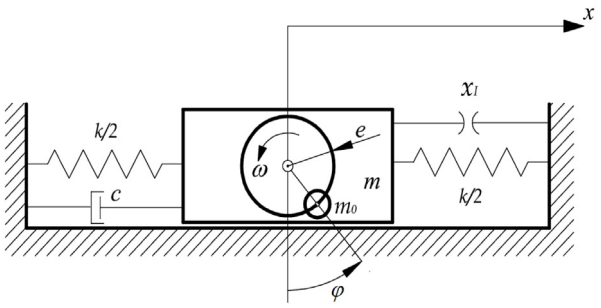

Fig. 1. The schematic representation of the experimental stand [20].

1. Experimental stand and its mathematical description

The study is based on the dynamical regimes observed on the experimental rig comprising an impacting oscillator. Since the rig has been already presented in detail in the reference [20], the present paper includes only give a short description. The experimental stand corresponds to the physical model presented in Fig. 1 and consists of a cart moving along a guide, integrated with a linear ball bearing and Hall effect sensors. The cart is mounted elastically with springs, and the external forcing is generated by a rotating unbalance mounted on a stepper motor with an encoder placed on the cart. The position of the moving body is limited by an obstacle placed on the support. The bumpers are made of steel and have locally, near the impact point, forms of balls of radii equal to 25 mm. Moreover, the centers of curvatures of both bumpers and the center of the contact point lie on one line parallel to the direction of motion of the cart.

The experimental data is collected and processed with the use of the National Instruments equipment and software. To describe the behavior of the mechanical system from Fig. 1, the mathematical model is developed first. It is assumed that the moving body has a total mass m and its position is described by the coordinate x. It is connected to the support by a linear spring with the total stiffness coefficient k. The position $x = 0$ corresponds to the resultant force in the springs equal to zero and a gap x_I between the two bumpers on the right side of the cart. The angular position of the disk mounted on the cart is equal to φ, while its angular velocity $\omega = \dot{\varphi}$ is assumed to be constant or varying very slowly. The unbalance m_0 is placed on the radius e of the disk.

As far as the description of the impact is concerned, it is worth mentioning that one can implement models assuming either hard impacts (instantaneous events), which are often based on the coefficient of restitution, or the so-called "soft" collisions. In the case of soft collisions, one should distinguish between mechanical systems with soft obstacles and systems with collisions between hard elements, usually modeled according to the Hertz model as locally deformable elements. The latter case has been considered in some recent works [8,9] and in our studies [20].

To describe the contact force during the impact with a compliant obstacle, a combination of a spring and a damper element (the Kelvin–Voigt viscoelastic model) is used. In order to avoid linear model's drawback related to the jump of the impact force at the beginning and the end of the contact, Hunt and Crossley [21] have proposed the nonlinear generalization of the linear model in the form $F = kh^{n_1} + bh^{n_2}\dot{h}^{n_3}$, where n_1, n_2, n_3 are some parameters, k is the stiffness coefficient, b is the damping coefficient, and h stands for the relative penetration depth.

The total component of resistance, proportional to velocity of both the spring and the linear bearing, is modeled in the form of a viscous damper with the coefficient c. It is also assumed that there exists some dry-friction-like component of resistance between the cart and the guide, inside the linear bearing, but it does not depend on normal load. The governing equations of the physical model take the following form

$$m\ddot{x} + kx + F_R(\dot{x}) + F_I(x, \dot{x}) = m_0 e\omega^2 \sin\varphi, \tag{1}$$

where the resistance force is described by the formula

$$F_R = c\dot{x} + T\frac{\dot{x}}{\sqrt{\dot{x}^2 + \varepsilon^2}},$$

whereas the impact force is $F_I = k_I((x - x_I)^{n_1} + b(x - x_I)^{n_2}\mathrm{sgn}\dot{x}|\dot{x}|^{n_3})$ for $x - x_I \geq 0$ and $(x - x_I)^{n_1} + b(x - x_I)^{n_2}\mathrm{sgn}\dot{x}|\dot{x}|^{n_3} \geq 0$, and $F_I = 0$ otherwise. In the work [20], the following set of parameters has been estimated or assumed a priori, leading to a good agreement between numerical simulations and experimental investigations: $m = 8.735$ kg, $m_0 e = 0.01805$ kg·m, $k = 1418.9$ N/m, $c = 6.6511$ N·s/m, $T = 0.63133$ N, $\varepsilon = 10^{-6}$ m/s, $k_I = 2.3983 \cdot 10^8$ N/m$^{3/2}$, $b = 0.8485$ m$^{-n_3}$ s^{n_3}, $n_1 = n_2 = 3/2$, $n_3 = 0.18667$. In the paper [20], the model (1) specified by this set of parameters is called the model BC and is the optimal one from a group of models tested in the work [20].

The comparison of experimental and numerical studies is presented in Fig. 2, which shows two bifurcation diagrams obtained numerically and experimentally for the obstacle position $x_I = -2.086 \cdot 10^{-3}$ m, based on Poincaré maps defined by sections $\varphi = 2\pi i$, $i = 1, 2, 3\ldots$. In the present study, the abovementioned parameters were used for the position of the limiter $x_I = -2.086 \cdot 10^{-3}$ m.

It should be mentioned that the paper [20] contains the description of experimental investigations of an oscillating system with impacts, the construction and validation of different mathematical models as well as bifurcation diagrams exhibiting the general properties of the observed oscillating regimes.

In the present research, we study the mathematical model which fits the experiment best. Moreover, we develop the tools for examining the attractors (especially chaotic), namely their statistic properties, with the use of the impact sequences. It turns out these sequences are extremely informative. In combination with their simple extraction from the physical model, the impact sequences can have great potential for future applications.

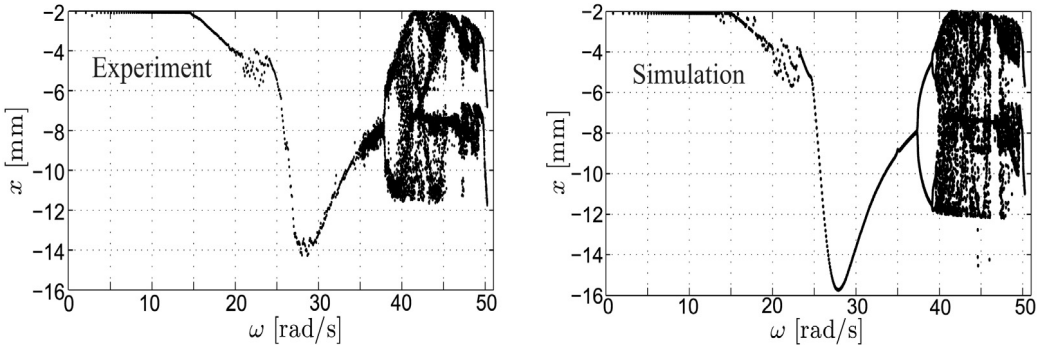

Fig. 2. Bifurcation diagrams obtained experimentally (left panel) and numerically (right panel) for increasing ω and the obstacle position $x_I = -2.086$ mm [20].

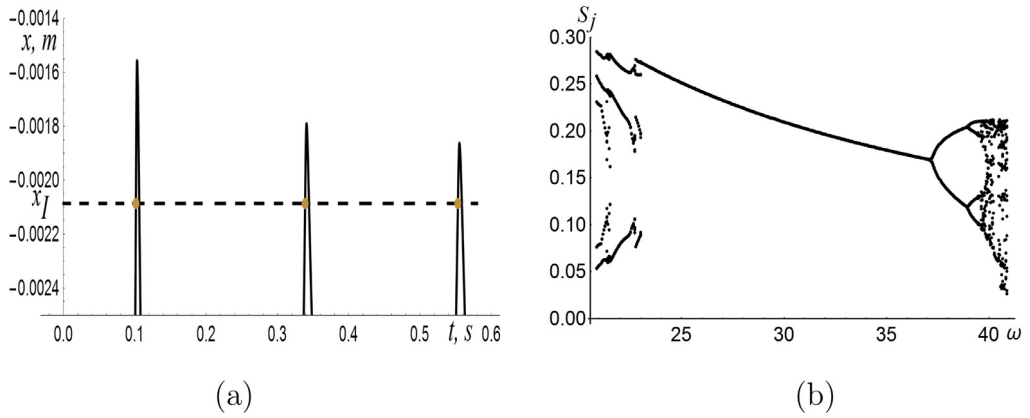

Fig. 3. The construction of the impact map and inter-impact intervals (a) and the bifurcation diagram for inter-impact intervals (b) at decreasing ω.

2. Studies of properties of attractors

In this section, we investigate the properties of attractors and their bifurcations via sequences of points generated by the stops impacts. These sequences form an impact map and can be regarded as a sort of Poincaré map. To construct the map, we analyze the profile of x component, observing the intersections of the increasing trajectory with the level $x = x_I$ (Fig. 3a). The time moments of impacts define the beginning of the collision and can be easily derived numerically.

As a result, the impact map can be extracted as a set of points $\{T_j : x(T_j) = x_I\}$ from the temporal profile of x during the numerical integration of the model (1). It is obvious that periodic regimes produce the periodic sequence $\{T_j\}$, whereas chaotic attractors generate stochastic sequences. These points define the inter-impact intervals $S_j = T_{j+1} - T_j$.

Using the impact map, the rearrangement of the phase space of Eq. (1) can be studied by means of the bifurcation diagram when model parameters vary. To make it, one can put the control parameter ω along the horizontal axis and the values of interval width S_j along the vertical one. The diagram obtained for the frequency ω decreasing from 40.86 rad/s is plotted in Fig. 3b.

From Fig. 3b it follows that reverse period doubling bifurcations occur at frequencies close to the initial $\omega = 40.86$ rad/s. The left part of the diagram exhibits a specific type of bifurcations met in the models with impacts. In particular, around $\omega = 23$ rad/s, additional branches of the bifurcation curve appear below the main curve corresponding to the limit cycle. In this case, we deal with the grazing bifurcation [10], when the trajectory touches the impact point with zero velocity as it is shown in the insets in Fig. 4. The phase portraits presented in Fig. 4 correspond to attractors just before the bifurcation at the external frequency $\omega = 23.05$ rad/s (Fig. 4a) and right after it, at $\omega = 23.03$ rad/s (Fig. 4b). Note that, according to Fourier spectral analysis, the former regime possesses the modes $\omega \cdot k$, $k = 1, 2, \ldots$, whereas in the latter regime, $\omega \cdot k$ is accompanied by $\omega_1 < \omega$ and combinational frequencies $\omega \cdot k \pm \omega_1$. As a result, one obtains a regime described by the quasiperiodic function nonlinearly dependent on two periodic functions of periods $2\pi/\omega$ and $2\pi/\omega_1$ [22].

2.1. Periodic regime

Let us now employ the impact map to study the properties of the periodic attractor existing at $\omega = 23.03$ rad/s (Fig. 4b). Let us integrate the model (1) over 100 s to get the sequence T_j containing 489 elements. Note that *Mathematica*'s procedure for capturing the curves intersections requires a specific value of MaxStepSize, i.e., MaxStepSize = 0.01 for a periodic sequence and MaxStepSize = 10^{-5} for chaotic impact trains in order to avoid omitting the impacts.

When constructing the sequence of impact intervals $\{S_j\}$ by the aforementioned method, one can arrange the successive iterations $S_{j+1} = f(S_j)$ (Fig. 5a).

In Fig. 5a it can be seen that only four different points are distinguished. This means that only four distinct intervals (or temporal scales) are present in the interval sequence. The histogram built for these points shows that the number of S_j of each width is equal. It is worth mentioning that, together with the analysis of the Fourier spectrum and the classical Poincaré section, the impact map allows one to supplement the information on the trajectory behavior. In particular, it is obvious that the sum of four arbitrary successive elements of S_j equals the period of the trajectory. In other words, the sum of four coordinates of the histogram bins gives 0.8184.

2.2. Chaotic regime

Consider the properties of the impact map in a chaotic regime when statistical features of the regime manifest clearly. Let us chose the case for $\omega = 40.86$ rad/s (period 0.154). Recall [20] that, after some transition time, the trajectory tends to the chaotic attractor, the phase portrait of which is depicted in Fig. 6a. The corresponding Fourier spectrum for this chaotic trajectory (Fig. 6b) possesses one substantial extremum at the frequency ω of forcing, whereas at smaller frequencies, the spectrum contains a dense set of excited frequencies. Also, an important characteristic of the chaotic regime is the Poincaré map coinciding with the set of points $x(t)$ in the section planes $\varphi = 2\pi i$, $i = 1, 2, \ldots$. Grouping them into the sequence $\{x_j; x_{j+1}\}$, we obtain Fig. 7a [20].

After rearranging the sequence S_i into the set $\{S_j; S_{j+1}\}$, a similar sequence can be constructed for the impact map (Fig. 7b). Both diagrams have a fractal nature, but the successive iterations form separated branches of the impact map. Note that a similar shape of the map is obtained in the for the return time map in the Rossler system [16] and the pendulum system from [18].

In this case, unlike the periodic regime, the sequence of points generated during the impacts is stochastic. Therefore, the statistic properties of these impacts train T_j are in question. Considering the number $N(t)$ of impacts in the time interval $(0, t)$, we lead to studying the distribution of N under the auxiliary assumptions: stationarity, independent increments and orderliness [23].

At first, let us check the stationarity of T_j. For this purpose, the number of impacts should be assessed at different intervals of time. We take the total time interval $t = 400$ s and divide it into five equal intervals. Counting the number of impacts in each time interval, one can obtain {572, 571, 579, 579, 574} impacts (the total number of impacts is 2875). Since the number of impacts is almost equal in all intervals, we can state that the process is *stationary*.

We also suppose that the number N depends only on the length of the time interval and impacts do not appear in groups, providing the implementation of other assumptions concerning the stochastic process.

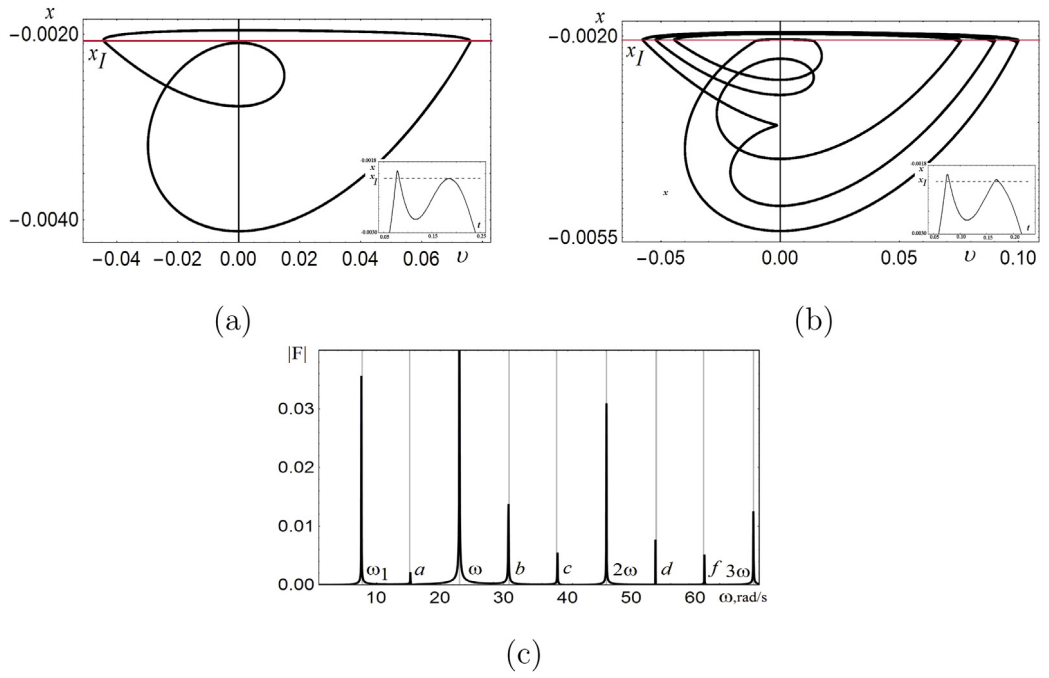

Fig. 4. The periodic trajectory at $\omega = 23.05$ rad/s just before the grazing bifurcation (a) and right after it (b). The insets show the parts of profiles where the grazing occurs. The Fourier spectrum (c) for the attractor depicted in panel (b). The symbols a, b, c, d, f designate the frequency combinations $\omega \pm \omega_1$, $2\omega \pm \omega_1$, and $3\omega - \omega_1$.

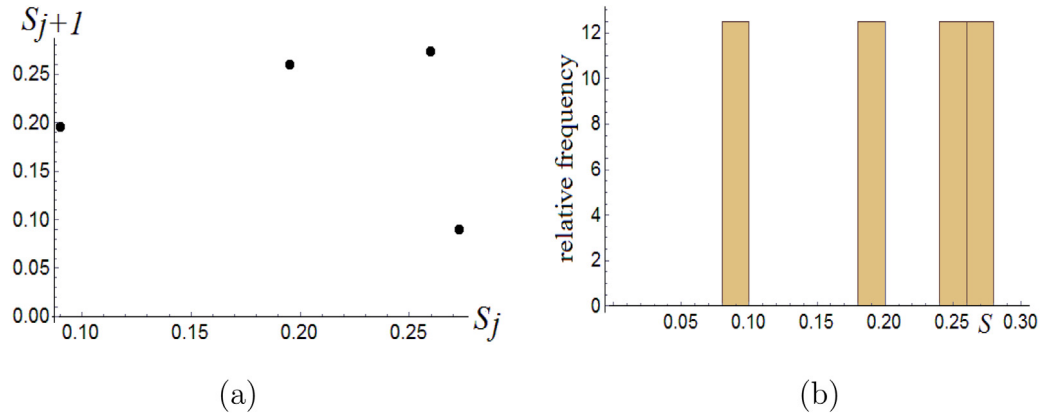

Fig. 5. Successive iterations (a) of the Poincaré return map for the periodic trajectory at $\omega = 23.05$ rad/s and the corresponding histogram (b).

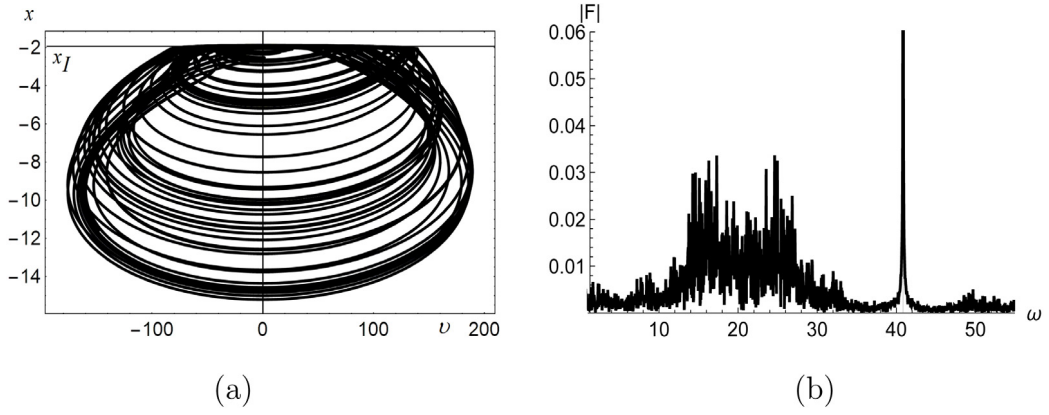

Fig. 6. The phase portrait (a) of the chaotic attractor and the corresponding Fourier spectrum (b) of the x-component.

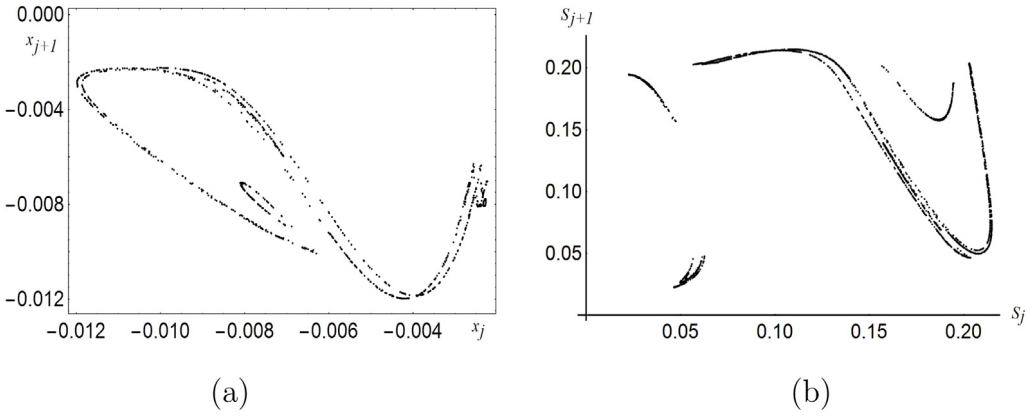

Fig. 7. Successive iterations of the Poincaré return map (a) and the impact map (b).

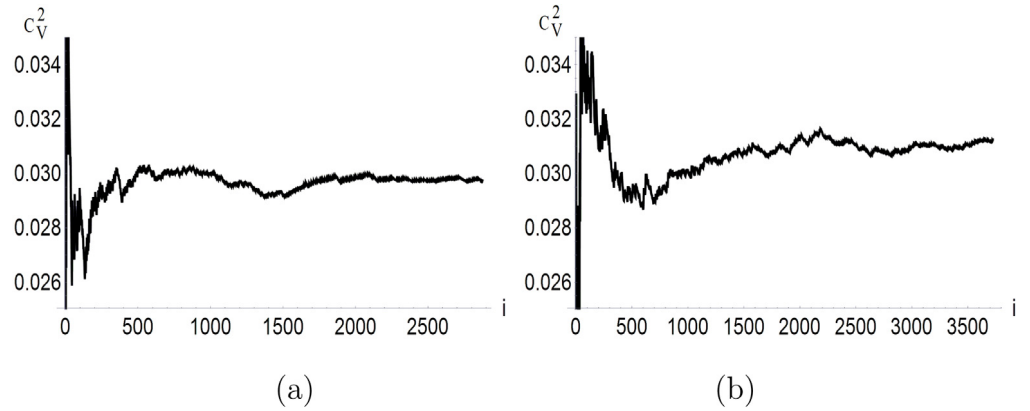

Fig. 8. The coefficient of variation C_V^2 for numerical (a) and experimental (b) models.

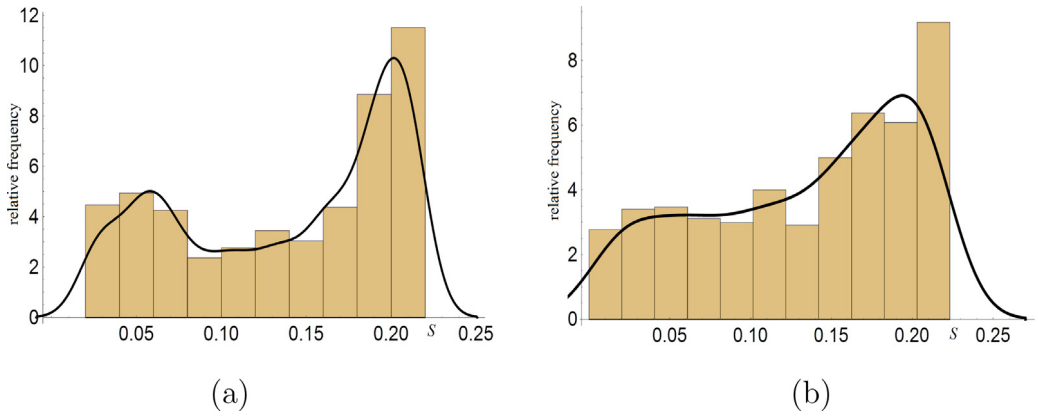

Fig. 9. The relative frequency histogram of inter-impact intervals and its smoothed version estimated numerically (a) and experimentally (b).

As it is well known, a random variable N having the aforementioned properties is described by the Poisson distribution

$$P(N(t) = n) = (\lambda t)^n \exp(-\lambda t)/n!,$$

where λ is the rate of Poisson process [23].

Note that many natural temporal processes obey this law, for instance, the number of earthquakes, β-particles after radioactive decay, spikes in neural activity. To define the type of distribution, it is useful to investigate the coefficient of variation C_V [13]

$$C_V^2 = \frac{D[N]}{M[N]}, \tag{2}$$

where $D[N]$ and $M[N]$ are the variance and the expected value of the variable N, respectively.

For the Poisson process, $C_V^2 = 1$ [23]. For the model (1), estimation of C_V^2 with the help of a sequence of inter-impact intervals results in Fig. 8a. It follows from the figure that for a large sample, the quantity C_V^2 tends to its limit value equal about 0.03. Since $C_V^2(i > 2000) < 1$, then the impact sequence behaves more regularly in comparison to the Poisson process [13].

The coefficient of variation C_V^2 is also derived for the experimental sample of inter-impact intervals (Fig. 8b). For large i, the profile of C_V^2 stabilizes in the vicinity of 0.03, that is a little bit higher than for the numerical inter-impact intervals. Nevertheless, the general conclusion

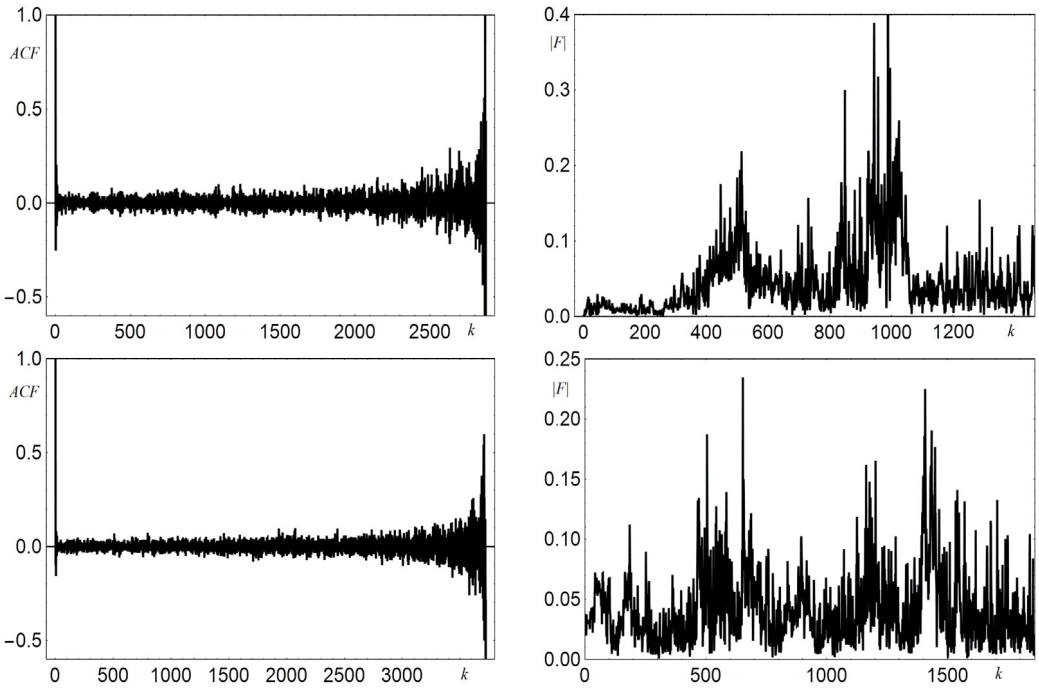

Fig. 10. The autocorrelation function (on the left) and its Fourier transform (on the right). The upper panels correspond to derivations of the numerical model, whereas the lower panels concern the experimental data.

on the similarity of behavior of both inter-impact intervals sequences is valid.

Let us consider the relative frequency histogram for inter-impact intervals, providing the estimation of a probability density function of a random variable, now. Using the proper tools of *Mathematica* software, we arrange 2875 intervals in ten bins and obtain the histogram as shown in Fig. 9a. The smooth line connecting the histogram bars clearly highlights two distinct maxima at points $T_1 = 0.05$ s and $T_2 = 0.2$ s. $T_{1,2}$ can relate to some temporal scales in the chaotic profile of x. Note that external forcing is characterized by the period $T = 2\pi/\omega = 0.15$ s which does not coincide with $T_{1,2}$. It is also worth noting that the histogram looks like a bimodal distribution, which can be often found in nature [16,24,25]. Until now, the problem of approximating the derived bimodal distribution has not been considered, although some progress has been achieved in this field [24]. Let us construct the relative frequency histogram (Fig. 9b) for the experimental data. This histogram possesses the substantial maximum for long intervals and weakly expressed extremum for short intervals. Therefore, the numerical and the experimental histograms have similar shapes. It should be noted that the experimental data contains noisy components. However, as it is shown in [25], incorporation of noise in time series leads to degeneration of a bimodal distribution into a unimodal one. Among important tools for analysis of noisy signals, one can mention studying the autocorrelation function (ACF) and its Fourier spectrum. Recall that the autocorrelation concerns the probability to find two impacts at a certain distance [13]. From the signal analysis theory, ACF defines the similarity of temporally lagged parts of a signal. Thus, the ACF is defined as follows

$$\mathrm{ACF}(k) = \frac{n}{n-k+1}\,\frac{\sum_{i=1}^{n-k+1}(S_i - \langle S\rangle)(S_{i-k+1} - \langle S\rangle)}{\sum_{i=1}^{n}(S_i - \langle S\rangle)^2}, \tag{3}$$

where $\langle S\rangle = \sum_{i=1}^{n} S_i/n$ is the mean value. With the use of the relation (3), we derive ACF and their Fourier transformations for inter-impact intervals obtained numerically (the upper panel in Fig. 10) and experimentally (the lower panel in Fig. 10). There are two peaks in the Fourier spectrum for the numerical inter-impact intervals and two weakly prevailing (due to the presence of noise) extrema in the experimental inter-impact intervals. These peaks can be associated with the temporal scales in the signal. In particular, the scales can be related to the intervals providing the maxima in the relative frequency histograms (Fig. 9).

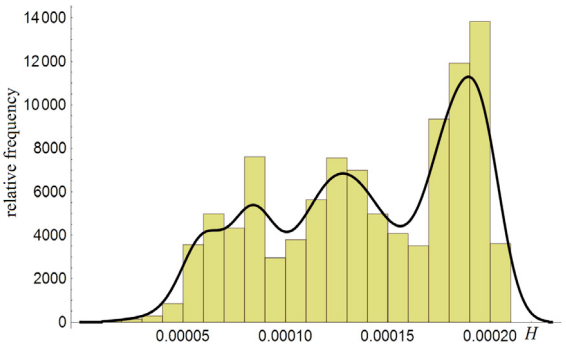

Fig. 11. The relative frequency histogram for the penetrations of the obstacle.

Analyzing the profile of x component in Fig. 3a, different heights of peaks (spikes above the level x_I) are observed. This tells us that the penetrations of the obstacle are different. Consider the distribution of a random variable H_j, which is a set of maximal values of obstacle penetrations during an impact. To derive the sequence H_j, we estimate the moments of time when the maximum of x is reached, i.e. $x'(t_j) = 0$ and $x(t_j) > x_I$. Then, $H_j = x(t_j) - x_I$. Let us form the relative frequency histogram of the corresponding values H_j. The resulting histogram presented in Fig. 11 possesses one essential maximum corresponding to the deepest penetration of the obstacle. There are also a few maxima almost twice smaller than the main peak. Thus, the observed distribution is not unimodal but multimodal.

3. Concluding remarks

We have studied the dynamics of the forced impacting oscillator by examining the sequences of impacts generated by stop impacts. It has been revealed that this quite simple mechanical system generates

extremely interesting impact trains, especially in the mode of chaotic vibrations. In the frequency domain, corresponding to the existence of periodic solutions, the characteristics of regimes and their bifurcations (in particular the grazing bifurcation) have been identified. When the chaotic regime occurs, the impact sequence is chaotic and is studied from the statistical point of view. At first, the construction of successive iterations of the impact map leads to the discontinuous locus of points corresponding to the beginning of impacts, unlike the classical Poincaré section for this model. Note also that the inter-impact intervals form the stationary non-Poissonian stochastic sequence and obey the bimodal distribution. A similar distribution is observed in the experimental data arranged in the histogram. The multimodal distribution is also revealed in the sequences of the obstacle penetration. The correlation analysis of these sequences has revealed the presence of temporal scales. All these features have been identified in both numerical and experimental investigations.

Acknowledgment

This work has been supported by the Polish National Science Centre, Poland under the grant OPUS 14 No. 2017/27/B/ST8/01330.

References

[1] R.I. Leine, H. Nijmeijer, Dynamics and Bifurcations of Non-Smooth Mechanical Systems, Springer, Berlin, 2004.
[2] J. Awrejcewicz, C.-H. Lamarque, Bifurcation and Chaos in Nonsmooth Mechanical Systems, World Scientific, London, 2003.
[3] A.S.E. Chong, Y. Yue, E. Pavlovskaia, M. Wiercigroch, Global dynamics of a harmonically excited oscillator with a play: Numerical studies, Int. J. Non-Linear Mech. 94 (2017) 98–108.
[4] T. Witelski, L.N. Virgin, C. George, A driven system of impacting pendulums: Experiments and simulations, J. Sound Vib. 333 (2014) 1734–1753.
[5] Y. Mikhlin, A. Vakakis, G. Salenger, Direct and inverse problems encountered in vibroimpact oscillations of a discrete system, J. Sound Vib. 216 (2) (1998) 227–250.
[6] S.W. Shaw, P.J. Holmes, A periodically forced piecewise linear oscillator, J. Sound Vib. 90 (1983) 129–155.
[7] F. Peterka, J. Vacik, Transition to chaotic motion in mechanical systems with impacts, J. Sound Vib. 154 (1992) 95–115.
[8] W. Serweta, A. Okolewski, B. Blazejczyk-Okolewska, K. Czolczynski, T. Kapitaniak, Lyapunov exponents of impact oscillators with Hertz's and Newton's contact models, Int. J. Mech. Sci. 89 (2014) 194–206.
[9] K. Czolczynski, A. Okolewski, B. Blazejczyk-Okolewska, Lyapunov exponents in discrete modelling of a cantilever beam impacting on a moving base, Int. J. Non-Linear Mech. 88 (2017) 74–84.
[10] W. Chin, E. Ott, H.E. Nusse, C. Grebogi, Grazing bifurcations in impact oscillators, Phys. Rev. E 50 (6) (1994) 4427–4444.
[11] X.-H. Long, G. Lin, B. Balachandran, Grazing bifurcations in an elastic structure excited by harmonic impactor motions, Physica D 237 (2008) 1129–1138.
[12] H.M. Isomaki, J. Von Boehm, R. Raty, Devil's attractors and chaos of a driven impact oscillator, Phys. Lett. A 107 (8) (1985) 343–346.
[13] W. Gerstner, W.M. Kistler, R. Naud, L. Paninski, Neuronal Dynamics: From Single Neurons to Networks and Models of Cognition, Cambridge University Press, Cambridge, 2014.
[14] D.M. Racicot, A. Longtin, Interspike interval attractors from chaotically driven neuron models, Physica D 104 (1997) 184–204.
[15] A.N. Pavlov, O.V. Sosnovtseva, E. Mosekilde, V.S. Anishchenko, Extracting dynamics from threshold-crossing interspike intervals: Possibilities and limitations, Phys. Rev. E 61 (5) (2000) 5033–5044.
[16] A.N. Pavlov, O.V. Sosnovtseva, E. Mosekilde, V.S. Anishchenko, Chaotic dynamics from interspike intervals, Phys. Rev. E 63 (2001) 036205.
[17] J.-Y. Lee, Motion behavior of impact oscillator, J. Marine Sci. Tech. 13 (2) (2005) 89–96.
[18] K.N. Slade, L.N. Virgin, P.V. Bayly, Extracting information from interimpact intervals in a mechanical oscillator, Phys. Rev. E 56 (3) (1997) 3705–3708.
[19] N.B. Janson, A.N. Pavlov, A.B. Neiman, V.S. Anishchenko, Reconstruction of dynamical and geometrical properties of chaotic attractors from threshold-crossing interspike intervals, Phys. Rev. E 58 (1) (1998) R4–R7.
[20] K. Witkowski, G. Kudra, G. Wasilewski, J. Awrejcewicz, Modelling and experimental validation of 1-degree-of-freedom impacting oscillator, J. Syst. Control Eng. (2018) 1–13.
[21] K. Hunt, E. Crossley, Coefficient of restitution interpreted as damping in vibroimpact, J. Appl. Mech. 42 (1975) 440–445.
[22] P. Berge, Y. Pomeau, C. Vidal, Order within Chaos: Towards a Deterministic Approach to Turbulence, Wiley-VCH, Weinheim, 1987.
[23] S. Ghahramani, Fundamentals of Probability, Prentice-Hall, Boca Raton, 2000.
[24] M.W. Levine, J.M. Shefner, A model for the variability of interspike intervals during sustained firing of a retinal neuron, Biophys. J. 19 (1977) 241–252.
[25] T. Sauer, Interspike interval embedding of chaotic signals, Chaos 5 (1995) 127–132.